

Properties of dense nuclear and neutron matter with relativistic nucleon-nucleon interactions

G. Q. Li* and R. Machleidt

Department of Physics, University of Idaho, Moscow, Idaho 83843

R. Brockmann

Department of Physics, University of Mainz, D-6500 Mainz, Germany

(Received 28 October 1991)

Within the framework of the Dirac-Brueckner (DB) approach, the properties of dense nuclear and neutron matter are investigated using realistic nucleon-nucleon (NN) interactions which are derived from relativistic meson-field theory and describe the two-nucleon system quantitatively. Single-particle potentials, equations of state, nucleon effective masses, Landau parameters, and speeds of sound are calculated and analyzed as functions of density, for both nuclear and neutron matter. In the DB approach, the equation of state comes out stiffer than in the most sophisticated nonrelativistic calculation, but softer than in the Walecka model. Possible extensions of the present approach to nucleon-nucleus scattering and nucleus-nucleus collisions are also discussed.

PACS number(s): 21.65.+f, 97.60.Jd, 21.30.+y

I. INTRODUCTION

One of the fundamental goals of theoretical nuclear physics is to explain consistently the properties of nuclear matter, finite nuclei, and nuclear reactions (nucleon-nucleus as well as nucleus-nucleus collisions) with one realistic nucleon-nucleon (NN) interaction that has a solid theoretical basis and describes the two-body system accurately. First attempts towards this aim were based on the simplest model for the atomic nucleus: nucleons obeying the nonrelativistic Schrödinger equation interact through a two-body potential that fits the low-energy NN scattering data and the properties of the deuteron. This work was done in the framework of Brueckner theory by solving the Bethe-Goldstone equation which yields an effective NN interaction in the medium [1–6]. Similar calculations have been performed in the framework of the variational method [7–9]. The predictions by this nonrelativistic model for nuclear saturation with a variety of NN interactions show a systematic behavior: in an energy versus density plot the saturation points are located along a band (“Coester band”) which does not meet the empirical area.

Many improvements of this simplest model have been proposed in order to overcome this difficulty. For example, meson and isobar degrees of freedom have been taken into account, in addition to the nucleon degree of freedom [10] (see Ref. [11] for a recent review). One of the most important developments in the extension of nuclear many-body theory is the replacement of the nonrelativistic Schrödinger equation with the relativistic Dirac equation to describe the single-particle motion in the medium [12–16]. This Dirac-Brueckner approach was inspired

by the success of the Dirac phenomenology for the properties of finite nuclei [17,18] as well as nucleon-nucleus scattering [19,20]. Indeed, when the Dirac-Brueckner method is used together with the one-boson-exchange (OBE) potential of the Bonn group [11,21], the empirical properties of nuclear matter are quantitatively reproduced [22]. (A comprehensive survey of the literature in the field of relativistic as well as nonrelativistic Brueckner and variational methods is given in Refs. [11,22].) An application of this approach to finite nuclei yielded also promising results [23]. It is thus reasonable to apply and extend this approach to other domains of nuclear physics.

An important application is the study of the properties of dense nuclear matter. These properties are important for particle physics, astrophysics, as well as nuclear physics. The nuclear equation of state, especially its incompressibility, is an important prerequisite for the study of the dynamic evolution of the early Universe and the stability of neutron stars [24,25]. Experimentally, intermediate-energy heavy-ion reactions offer the unique opportunity to obtain a piece of dense nuclear matter in the laboratory. However, for the analysis of these reactions the properties of nuclear matter at high density are needed which can only be obtained from theoretical investigations [26,27]. For example, in the calculation of meson production cross sections in heavy-ion reactions, one needs the meson-baryon interaction in the dense medium in order to estimate the reabsorption of the primordial mesons by the baryons [28–30]. In this sense, the theoretical investigation of the properties of dense nuclear matter, as well as the properties of hadrons in the dense medium [31], is of great importance.

There exist some phenomenological investigations of the properties of dense nuclear matter, e.g., in the framework of the Walecka model [32–34]. It is an empirical model in the sense that it contains free parameters which are adjusted to fit the saturation properties of nuclear

*Permanent address: Department of Physics, Hangzhou University, Hangzhou 310028, P.R. China.

matter. Thus, the connection to the underlying realistic (bare) NN interaction is lost.

Another important topic is the properties of dense neutron matter which are useful in the study of supernovae and neutron stars. There are calculations of the properties of neutron matter within the Walecka model; the resulting equation of state has been used to study the structure and stability of neutron stars [35–37]. It is also of interest to study the properties of neutron matter based on realistic NN interactions.

The purpose of the present paper is to study the properties of nuclear matter and neutron matter in the framework of the Dirac-Brueckner approach with the relativistic meson-theoretic potential of the Bonn group. Previous discussions of the properties of nuclear matter are frequently expressed in terms of the Fermi momentum of the system. Since the ultimate goal of the present study is to connect the realistic NN interaction with heavy-ion reactions where the density of the system rather than the Fermi momentum is considered as a relevant quantity, we will present our results in terms of density of nuclear matter or neutron matter. In Sec. II we give a brief description of the theoretical formalism. The results and discussion are presented in Sec. III. Finally, in Sec. IV we give our summary and outlook including a discussion of possible extensions of the present approach to nucleon-nucleus scattering as well as nucleus-nucleus collisions.

II. SKETCH OF FORMALISM

The relativistic OBE potential to be used in the Dirac-Brueckner calculation is constructed in the framework of the covariant Thompson equation [38] which is a three-dimensional reduction of the Bethe-Salpeter equation [39]. In the center-of-mass (c.m.) system of the two interacting nucleons, the Thompson equation has the following form:

$$\begin{aligned} \mathcal{T}(\mathbf{q}', \mathbf{q}) = & V(\mathbf{q}', \mathbf{q}) \\ & + \int \frac{d^3k}{(2\pi)^3} V(\mathbf{q}', \mathbf{k}) \frac{m^2}{E_k^2} \frac{1}{2E_q - 2E_k + i\xi} \\ & \times \mathcal{T}(\mathbf{k}, \mathbf{q}), \end{aligned} \quad (1)$$

where m denotes the mass of the nucleon and $E_k = (\mathbf{k}^2 + m^2)^{1/2}$.

The OBE potential is defined as the sum of one-particle-exchange amplitudes of certain bosons with given mass and coupling. Usually six nonstrange bosons with mass below 1 GeV are used. The pseudovector (derivative/gradient) coupling, instead of pseudoscalar coupling is used for the pseudoscalar bosons (π and η) in order to avoid unphysically large antiparticle contributions. The details about the derivation of the OBE potential, the parameters (mass, coupling constant, and cutoff of the bosons) and the description of the two-body system have been extensively discussed in Refs. [11,21,22,40]. Three parameter sets, usually denoted by Bonn A, B, and C, have been proposed and used in various calculations of finite nuclei and nuclear matter [11,22,23]. In Table I we show the predictions of these potentials for the energies of ${}^3\text{H}$ and ${}^{16}\text{O}$ as well as for the saturation properties of nuclear matter. Also shown in the table are the predictions of a sophisticated nonrelativistic variational calculation [9], the Walecka model [34] and experiment. It is seen that the Bonn A potential gives an extremely good agreement with the experimental data. The essential difference between the three potentials Bonn A, B, and C is the strength of the tensor force as reflected in their predictions for the D -state probability of the deuteron ($P_D = 4.5, 5.1, 5.5\%$ for A,B,C, respectively). This strength of the nuclear tensor force is not determined well by present NN data.

When two nucleons scatter from each other in nuclear matter, the medium effects, such as the Pauli blocking for the intermediate states and the density dependence of the nucleon effective mass due to nucleon self-energy, should be taken into account in the Thompson equation describing this process. As in the nonrelativistic case, one starts from a bare interaction and carries out a Brueckner calculation to get the effective interaction, often denoted as G matrix, in the medium. The properties of the nuclear system are then derived from this effective interaction. In the relativistic treatment, the Dirac equation is used for the description of the single-particle motion in the medium (hence the name of Dirac-Brueckner approach):

$$[\boldsymbol{\alpha} \cdot \mathbf{p} + \beta(m + U_S) + U_V] \bar{u}(\mathbf{p}, s) = \bar{\epsilon}_p \bar{u}(\mathbf{p}, s), \quad (2)$$

TABLE I. Energy of ${}^3\text{H}$ and energy per nucleon of ${}^{16}\text{O}$ and saturation properties of nuclear matter from various calculations and from experiment. For nuclear matter the saturation energy per nucleon, \mathcal{E}/A , the saturation density, ρ , and the compression modulus, K , are given. DBHF stands for Dirac-Brueckner-Hartree-Fock calculation.

Model	Calculational method	${}^3\text{H}$ (MeV)	${}^{16}\text{O}$ (MeV)	Nuclear saturation \mathcal{E}/A (MeV)	Matter properties ρ (fm^{-3})	K (MeV)	Ref.
Bonn A	34-channel Faddeev DBHF	-8.32	-7.08	-15.59	0.185	290	[11] [22,23]
Bonn B	34-channel Faddeev DBHF	-8.13	-5.84	-13.60	0.174	249	[11] [22,23]
Bonn C	34-channel Faddeev DBHF	-7.99	-4.95	-12.26	0.155	185	[11] [22,23]
AV14+UVII	Variational	-8.8	-7.8	-12.4	0.194	209	[9]
Walecka	Mean field	-8.8	-7.8	-12.4	0.194	209	[9]
	Experiment	-8.48	-7.98	-16.0 \pm 1.0	0.17 \pm 0.02	2.10 \pm 30	[11]

where U_S is an attractive scalar field and U_V is (the timelike/fourth component of) a repulsive vector field. They are determined self-consistently from the realistic NN interaction used in the Dirac-Brueckner calculation.

In the nuclear medium, a Dirac mass \tilde{m} is introduced

$$\tilde{m} = m + U_S, \quad (3)$$

which is density dependent through the density dependence of the self-consistent potential U_S . Furthermore it is useful to define a quasienergy \tilde{E}_p by

$$\tilde{E}_p = (\mathbf{p}^2 + \tilde{m}^2)^{1/2}. \quad (4)$$

With this we can write

$$\tilde{\epsilon}_p = \tilde{E}_p + U_V.$$

The G matrix can be directly obtained in the nuclear matter rest frame from the Thompson equation in the medium [22]:

$$\begin{aligned} \tilde{G}(\mathbf{q}', \mathbf{q} | \mathbf{P}, \bar{z}) &= \tilde{V}(\mathbf{q}', \mathbf{q}) \\ &+ \int \frac{d^3k}{(2\pi)^3} \tilde{V}(\mathbf{q}', \mathbf{k}) \frac{\tilde{m}^2}{\tilde{E}_{(1/2)\mathbf{P}+\mathbf{k}}^2} \\ &\times \frac{Q(\mathbf{k}, \mathbf{P})}{\bar{z} - 2\tilde{E}_{(1/2)\mathbf{P}+\mathbf{k}}} \tilde{G}(\mathbf{k}, \mathbf{q} | \mathbf{P}, \bar{z}), \quad (5) \end{aligned}$$

with

$$\bar{z} = 2\tilde{E}_{(1/2)\mathbf{P}+\mathbf{q}}.$$

\mathbf{P} is the c.m. momentum of the two colliding nucleons in the nuclear medium. The essential difference between the free-space Thompson equation [Eq. (1)] and the Thompson equation in the medium [Eq. (5)] is the inclusion of the Pauli operator $Q(\mathbf{k}, \mathbf{P})$ and the use of a density-dependent effective mass \tilde{m} in the latter case.

From the G matrix the single-particle potential is obtained:

$$U_i = \text{Re} \sum_{j \leq k_F} \frac{\tilde{m}^2}{\tilde{E}_i \tilde{E}_j} \langle ij | \tilde{G}(\bar{z}) | ij - ji \rangle. \quad (6)$$

This single-particle potential is related to the scalar and vector potentials in the Dirac equation by

$$U_i = \frac{\tilde{m}}{\tilde{E}_i} U_S + U_V. \quad (7)$$

Equation (5) is decomposed into partial waves and solved in momentum space by means of the matrix inversion method of Ref. [41]. The self-consistent potentials U_S and U_V are determined from Eqs. (5)–(7) by an iterative procedure: Starting from reasonable initial values for $U_S^{(0)}$ and $U_V^{(0)}$, one solves the Thompson equation with the use of a realistic NN interaction to get the G matrix which leads to a new set of values for $U_S^{(1)}$ and $U_V^{(1)}$ to be used in the next iteration. This procedure continues until the desired accuracy for the self-consistent potential is achieved. Since the numerical calculation is carried out directly in the nuclear matter rest frame, a cumbersome relativistic transformation between the two-nucleon c.m.

system and the nuclear matter rest frame is avoided. Thus, the present approach can be straightforwardly extended to the case of nucleus-nucleus collisions where the c.m. system of the two colliding nuclei shall be used.

III. RESULTS AND DISCUSSION

A. Nuclear matter

Nuclear matter is an infinite uniform system of nucleons interacting via the strong force without electromagnetic interactions. It is supposed to approximate conditions in the interior of a heavy nucleus. In this subsection we will present our results for the properties of symmetric nuclear matter (equal number of protons and neutrons).

1. Single-particle potentials

As in the phenomenological Walecka model, the essential quantities in the Dirac-Brueckner calculation are the scalar potential U_S and the timelike component of the vector potential U_V , which are determined self-consistently from a given bare NN interaction by an iterative procedure. These potentials are often denoted as Dirac potentials. We show in Fig. 1 the variation of the Dirac potentials U_S and U_V with nuclear matter density. The solid, dashed, and dotted curves correspond to the results obtained with the Bonn A, B, and C potentials, respectively. We see in the figure that both U_S and U_V are strongly density dependent. While U_V increases almost linearly with the density, the decrease of U_S is slower at

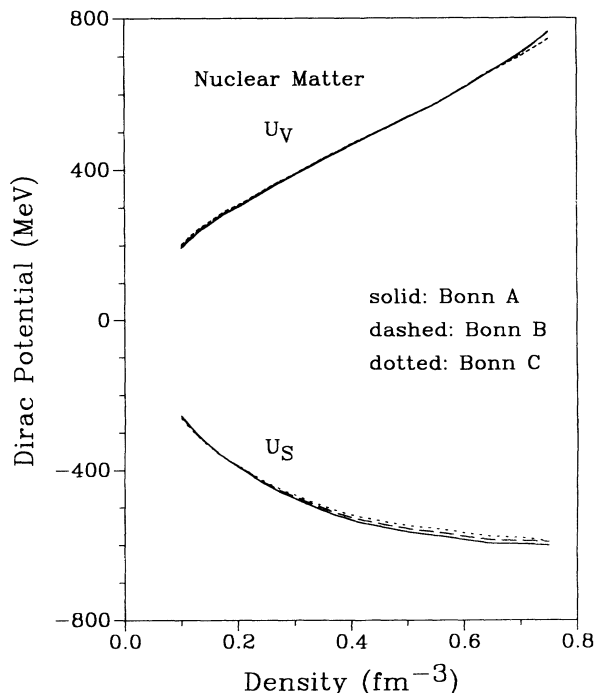


FIG. 1. The variation of the Dirac potentials with density. The solid, dashed, and dotted curves represent the results derived from the Bonn A, B, and C potentials, respectively.

higher density. This provides the mechanism by which the Dirac-Brueckner calculations reproduce quantitatively the saturation properties of nuclear matter, as shown in Ref. [22]. We also notice that, while the vector poten-

tial U_V is almost independent of the OBE parameter sets used, the scalar potentials U_S corresponding to different parameter sets do show some difference, especially at higher density. The Bonn A potential, which has the weakest tensor component, results in the most attractive potential. This is the reason why the Bonn A potential leads to a larger binding energy for nuclear matter than

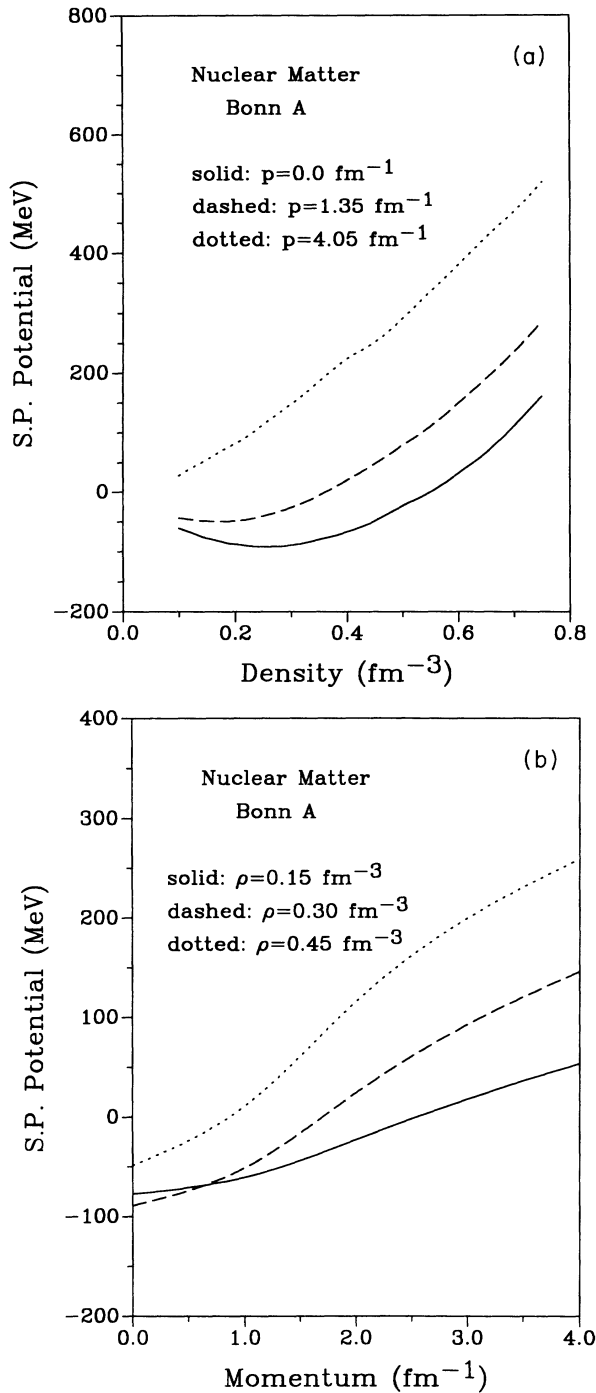


FIG. 2. (a) The variation of the single-particle potentials with density. The solid, dashed, and dotted curves represent the single-particle potential of particles with momentum 0, 1.35, and 4.05 fm^{-1} , respectively. (b) The variation of the single-particle potentials with momentum. The solid, dashed, and dotted curves represent three cases with nucleon density $\rho=0.15$, 0.30 , and 0.45 fm^{-3} , respectively.

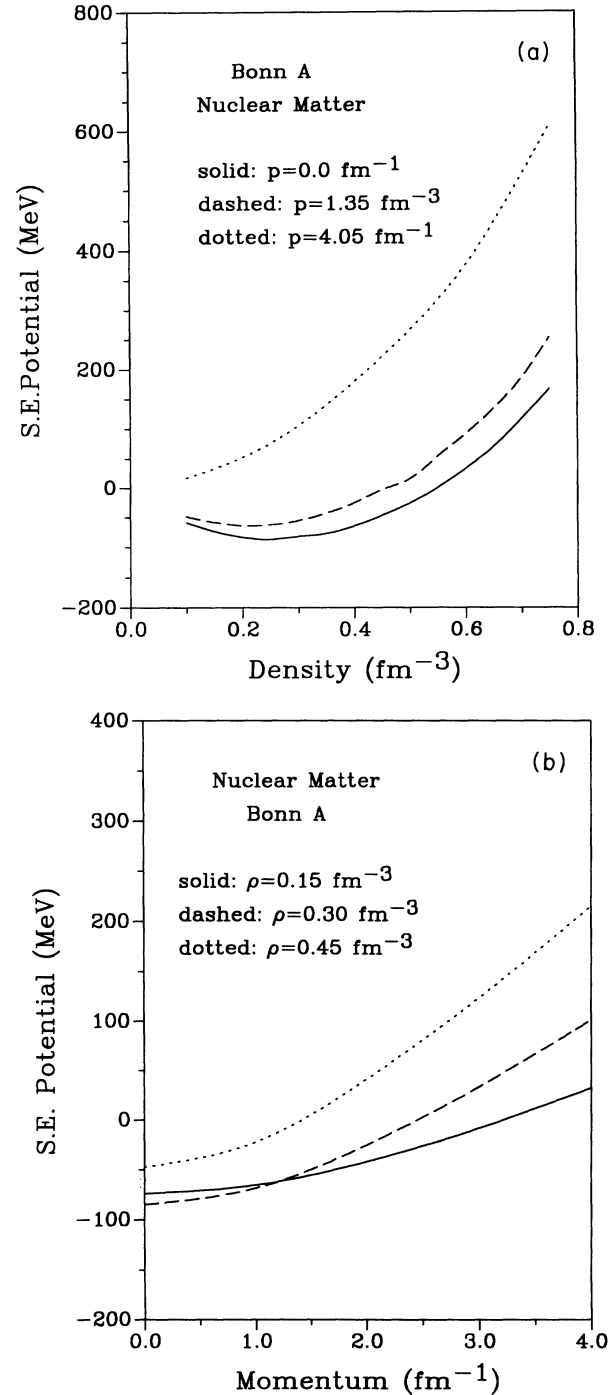


FIG. 3. (a) The same as Fig. 2(a), but for the Schrödinger-equivalent potentials. (b) The same as Fig. 2(b), but for the Schrödinger-equivalent potentials.

the other two parameter sets [22].

With the self-consistently determined Dirac potentials, we can readily calculate the single-particle potential $U_{s.p.}$:

$$U_{s.p.} = \frac{\tilde{m}}{(\mathbf{p}^2 + \tilde{m}^2)^{1/2}} U_S + U_V, \quad (8)$$

where \mathbf{p} is the momentum of the particle in the nuclear matter rest frame. Obviously the single-particle potential is density and momentum dependent.

A quantity of practical importance is the so-called Schrödinger-equivalent potential $U_{s.e.}$ which is often used in the Dirac phenomenology for nucleon-nucleus scattering [42]. Equation (2) implies the following energy-momentum relation:

$$\mathbf{p}^2 + (m + U_S)^2 = (\varepsilon + m - U_V)^2 \quad (9)$$

where we use $\tilde{\varepsilon}_p = \varepsilon + m$ with ε the single-particle energy. Equation (9) can be written in the following Schrödinger-type form [43]:

$$\frac{\mathbf{p}^2}{2m} + U_{s.e.} = \varepsilon + \frac{\varepsilon^2}{2m}$$

with the Schrödinger-equivalent potential, $U_{s.e.}$, defined as

$$U_{s.e.}(\varepsilon) = U_S + U_V + \frac{\varepsilon}{m} U_V + \frac{1}{2m} (U_S^2 - U_V^2). \quad (10)$$

This quantity is also momentum and density dependent.

The single-particle potential $U_{s.p.}$ and the Schrödinger-equivalent potential $U_{s.e.}$, thus obtained, are shown in Fig. 2(a) and Fig. 3(a) as functions of nuclear matter density, and in Fig. 2(b) and Fig. 3(b) as functions of particle momentum. The results have been obtained by using the Bonn A potential. In Fig. 2(a) and Fig. 3(a) we present three different results corresponding to particles with momentum 0 (solid curve), 1.35 fm^{-1} (dashed curve), and 4.05 fm^{-1} (dotted curve), while in Fig. 2(b) and Fig. 3(b) we show three different results corresponding to nucleon matter density $\rho = 0.15 \text{ fm}^{-3}$ (solid curve), 0.30 fm^{-3} (dashed curve), and 0.45 fm^{-3} (dotted curve). The variations of $U_{s.p.}$ and $U_{s.e.}$ with momentum and density are about the same. At low momentum, the potentials first decrease and then increase with density, while at high momentum, the potentials are monotonously increasing functions of the density. The introduction of a Schrödinger-equivalent potential in the Dirac-Brueckner approach is of practical relevance when the approach is used to study nucleon-nucleus scattering. It is also useful for an unambiguous definition of the nucleon effective mass in a relativistic framework, as we will discuss below.

2. Equation of state

The energy per nucleon as a function of the density of the system is often referred to as the nuclear equation of state. Note that this differs from the more common definition of an equation of state which is the variation of the system pressure with its density. In the Dirac-

Brueckner approach, the energy per nucleon, \mathcal{E}/A , is obtained from the G matrix of Eq. (5):

$$\frac{\mathcal{E}}{A} = \frac{1}{A} \sum_{i \leq k_F} \frac{m\tilde{m} + \mathbf{p}_i^2}{\tilde{E}_i} + \frac{1}{2A} \sum_{i,j \leq k_F} \frac{\tilde{m}^2}{\tilde{E}_i \tilde{E}_j} \langle ij | \tilde{G}(\tilde{z}) | ij - ji \rangle - m, \quad (11)$$

where

$$\tilde{z} = \tilde{E}_i + \tilde{E}_j.$$

The present result for the microscopic nuclear equation of state, obtained in the Dirac-Brueckner approach with the OBE potentials, are shown in Figs. 4(a) and 4(b). In addition we list in Table II the energy per nucleon, \mathcal{E}/A , of nuclear matter and neutron matter as function of density, as obtained in the Dirac-Brueckner calculation with the Bonn A potential. In Fig. 4(a) the solid, dashed, and dotted curves represent our results corresponding to Bonn A, B, and C, respectively. The shaded area indicates the empirical saturation region of normal nuclear matter. The two solid curves marked with squares and circles correspond to Skyrme parametrizations for the nuclear equation of state which is frequently used in the theoretical description of intermediate-energy heavy-ion reactions [26–30]. The one with circles is the so-called soft equation of state with an incompressibility (at the saturation point) $K = 200 \text{ MeV}$, while the one with squares represents the so-called stiff equation of state with the incompressibility (at the saturation point) $K = 380 \text{ MeV}$. In Fig. 4(b) the equation of state corresponding to the Bonn A potential (solid curve) is compared with the predictions by the Walecka model (dashed curve) [34] and by the most sophisticated nonrelativistic

TABLE II. Energy per nucleon in nuclear and neutron matter as a function of density for the Bonn A potential as obtained in a Dirac-Brueckner calculation.

$\rho \text{ (fm}^{-3}\text{)}$	$\mathcal{E}/A \text{ (MeV)}$	
	Nuclear matter	Neutron matter
0.10	-12.54	10.15
0.13	-14.07	12.62
0.15	-14.07	14.55
0.16	-15.20	15.54
0.17	-15.40	16.63
0.18	-15.54	17.81
0.20	-15.51	20.47
0.25	-13.81	28.48
0.30	-9.68	39.23
0.35	-3.31	52.91
0.40	5.61	69.26
0.45	16.44	86.89
0.50	29.68	106.34
0.55	44.62	126.24
0.60	61.77	147.31
0.65	80.94	170.14
0.70	99.61	196.57
0.75	119.93	230.13

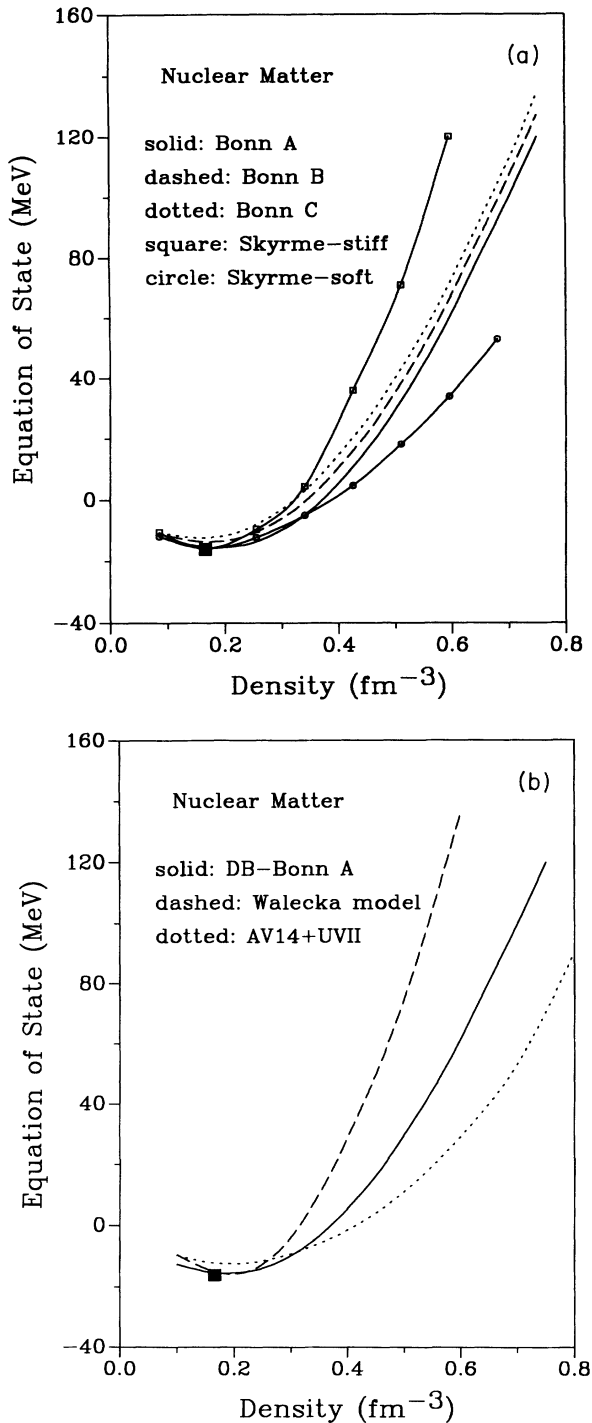


FIG. 4. (a) The equation of state, the energy per nucleon, of nuclear matter. The solid, dashed, and dotted curves are the present results corresponding to Bonn A, B, and C potentials, respectively. The solid curves with circles and squares represent the soft and stiff equations of state of the Skyrme parametrization. The solid square indicates the empirical saturation region of normal nuclear matter. (b) The equation of state obtained in Dirac-Brueckner calculation with Bonn A potential (solid curve) is compared with that of the Walecka model [34] (dashed curve) and that of a nonrelativistic calculation (dotted curve) [9]. The solid square indicates the empirical saturation region of normal nuclear matter.

calculation (dotted curve) [9]. In the latter calculation, the Argonne V14 two-nucleon potential together with the Urbana VII three-nucleon force is used in a variational method.

From these figures, three observations can be made: (1) Of the three potentials, Bonn A, which has the weakest tensor force, gives the best fit of the empirical saturation properties of normal nuclear matter. Bonn B and C underestimate the binding energy by about 10%. Further results concerning the properties of nuclear matter and neutron matter will, therefore, be given for the Bonn A potential only. (2) Our equation of state is softer than that of the Walecka model, but stiffer than the prediction of the nonrelativistic approach, even though in the latter approach a three-nucleon potential is taken into account. This “intermediate” position of our result in Fig. 4(b) qualifies our prediction as very reasonable. The nonrelativistic calculation of Ref. [9] saturates nuclear matter at too high a density (cf. Table I). Thus, this model still lacks density-dependent repulsion. The Walecka model, on the other hand, does saturate nuclear matter correctly, however, at the expense of far too high a compressibility of about 540 MeV (cf. Table I). Our model (DB with Bonn A) predicts nuclear matter saturation correctly and the compressibility reasonably close to empirical information. The unrealistic stiffness of the Walecka model can be attributed to the neglect of two-nucleon correlations [14,33]. (3) Around the saturation point, the microscopic equation of state derived from the Bonn A potential agrees with the phenomenological equations of state of the Skyrme parametrization. At high density, large differences occur between the microscopic and phenomenological equations of state. However, it is remarkable that the microscopic one lies in between the phenomenological soft and hard equations of state. It will be of practical interest to apply the microscopic equation of state based on the realistic NN interaction in the theoretical description of heavy-ion reactions, which constitutes one of the ultimate goals of the present study.

3. Effective masses

The introduction of the nucleon effective mass is a convenient way to describe the motion of nucleons in the nuclear medium. It reflects the influence of the mean field (optical potential) on the nucleon motion. In the nonrelativistic theory, the microscopic mean field (optical potential) \mathcal{V}_s is in general nonlocal and energy dependent. The effective mass is defined in such a way that it characterizes the energy dependence of a *local* potential V_s which is equivalent to the nonlocal microscopic potential \mathcal{V}_s [43]:

$$\frac{m^*}{m} = 1 - \frac{d}{d\epsilon} V_s(\epsilon). \quad (12)$$

The empirical value for the effective mass in nuclear matter derived from the analysis of experimental data in the framework of nonrelativistic shell or optical models is [43,44]

$$\frac{m^*}{m} \approx 0.7 - 0.8. \quad (13)$$

In the relativistic treatment of nuclear problems, the concept of “effective mass” is also frequently adopted. However, in this case the term usually denotes different quantities under different circumstance. In Ref. [43] a clarification of the relativistic definition of the effective mass is given. A quantity that is often referred to as “effective mass” in the relativistic approach is the tilded mass \tilde{m} which we introduced in Eq. (3). In Refs. [43,45] this mass is called “Dirac mass,” a term we adopt in this paper. Since its definition has no apparent relation to the nonrelativistic definition of the effective mass, Eq. (12), the Dirac mass should not be compared to the empirical value of Eq. (13) and this wrong comparison should not be considered as a judgement for the relativistic theory itself, or for the underlying bare NN interaction used in the theory.

The introduction of the Schrödinger-equivalent potential $U_{S.e.}$ in the relativistic approach makes it possible to define an effective mass which is analogous to Eq. (12):

$$\frac{m^*}{m} = 1 - \frac{d}{d\epsilon} U_{S.e.}(\epsilon) = 1 - \frac{U_V}{m}. \quad (14)$$

It is this quantity that should be compared with the empirical value of Eq. (13).

Another quantity, sometimes also known as “effective mass,” is the Landau mass m_L^* which gives a measure of the density of states in the vicinity of the Fermi level. It can be defined with the help of the dispersion relation, Eq. (9) [43,46,47]:

$$\frac{m_L^*}{m} = \frac{k_F}{m} \left[\frac{dp}{d\epsilon} \right]_{k_F} = \frac{(k_F^2 + \tilde{m}^2)^{1/2}}{m}. \quad (15)$$

m_L^* plays the role of the “effective mass” of the nonrelativistic Landau theory. However it should not be identified with the effective mass defined in Eq. (14).

The comparison of these “effective masses” is presented in Fig. 5, where \tilde{m} , m^* , and m_L^* are plotted as functions of the density of nuclear matter. Solid, long-dashed, and short-dashed curves correspond to Dirac mass \tilde{m} , effective mass m^* , and Landau mass m_L^* , respectively. The Bonn A potential is used in this calculation. The dotted curve in the figure represents the Dirac mass of the Walecka model [34]. The dagger in the figure indicates the empirical values for the effective mass which are obtained in the analyses of experimental data in the nonrelativistic shell or optical model [Eq. (13)]. It is a great success of our Dirac-Brueckner approach that the effective mass (the long-dashed curve) obtained in the present calculation is very close to the empirical value of Eq. (13). Thus the Bonn A potential reproduces not only the saturation density and the binding energy, but also the nucleon effective mass. Earlier conjectures that the Dirac-Brueckner approach underestimates the nucleon effective mass were obviously wrong and due solely to a misidentification of the relativistic and nonrelativistic definitions for the effective mass. Clear difference is seen between the Dirac mass in the present approach and that of the Walecka model. The Dirac mass in the latter case decreases much faster with increasing density.

The variations of the three “effective masses” with den-

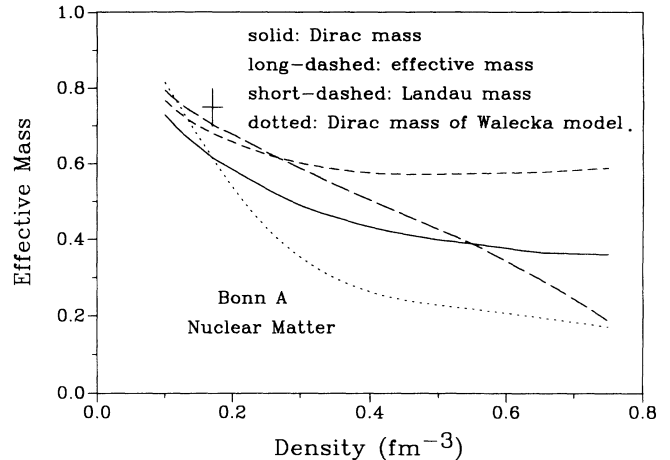


FIG. 5. The variation of “effective masses” (in unit of m) with density. The solid, long-dashed, and short-dashed curves correspond to the Dirac mass, effective mass, and Landau mass, respectively. The dotted curve is the Dirac mass in the Walecka model. The dagger denotes the empirical value of the effective mass [43,44].

sity are not the same. At low density, the effective mass m^* has the largest value, it decreases almost linearly with density, since the vector potential U_V increases with density linearly (Fig. 1). The Dirac mass \tilde{m} also decreases with density. But at higher density it decreases slower, since the scalar potential U_S decreases slower at higher density. On the other hand, the Landau mass m_L^* first decreases with density and then at high density it increases with the density. m_L^* is composed of two parts which have opposite behavior as functions of density: the Fermi momentum k_F increases with density while the Dirac mass \tilde{m} decreases. At extremely high density, m_L^* approaches k_F .

4. Landau parameters

Landau theory provides a practical way of describing an interacting fermion system, since there is a one-to-one correspondence between the single-particle states of the noninteracting system and the quasiparticle states of the interacting system. The quasiparticle-quasihole interaction $f(\mathbf{p}, \mathbf{p}')$ is defined to be the second derivative of the energy functional with respect to the occupation function [46,47]. It can be expanded according to its spin-isospin content:

$$f(\mathbf{p}, \mathbf{p}') = F(\mathbf{p}, \mathbf{p}') + F'(\mathbf{p}, \mathbf{p}') \boldsymbol{\tau} \cdot \boldsymbol{\tau}' + G(\mathbf{p}, \mathbf{p}') \boldsymbol{\sigma} \cdot \boldsymbol{\sigma}' + G'(\mathbf{p}, \mathbf{p}') \boldsymbol{\sigma} \cdot \boldsymbol{\sigma}' \boldsymbol{\tau} \cdot \boldsymbol{\tau}'. \quad (16)$$

If one restricts the consideration to single-particle states in the vicinity of the Fermi level, then the interaction depends only on the angle θ between \mathbf{p} and \mathbf{p}' . This suggests an expansion in terms of Legendre polynomials, e.g.,

$$F(\mathbf{p}, \mathbf{p}') = \sum_l F_l P_l(\cos \theta).$$

The constants F_l are called Landau parameters. More frequently one introduces the dimensionless Landau parameter f_l by defining

$$F_l = C f_l,$$

where C is the inverse density of states at the Fermi surface [47]:

$$C^{-1} = \left(\frac{\partial p}{\partial \epsilon} \right)_{k_F} \frac{2k_F^2}{\pi^2}.$$

In the relativistic case, the explicit form of the inverse density of state is given by [12,47]

$$C^{-1} = \frac{2k_F(k_F^2 + \bar{m}^2)^{1/2}}{\pi^2}. \quad (17)$$

It is instructive to relate these Landau parameters, which are important for the phenomenological description of nuclear properties, to the underlying realistic NN interaction. The Landau parameters for $l=0$, f_0 , f'_0 , g_0 , and g'_0 , are easily obtained in our self-consistent Dirac-Brueckner calculation. In Ref. [22], a nonrelativistic expression for the inverse density of states, mk_F/π^2 , was used. In order to be more consistent, the results presented in this paper have been obtained with the relativistic inverse density of states, Eq. (17).

Another important Landau parameter, f_1 , can be easily obtained from the Landau mass m_L^* [43]:

$$m_L^* = [(k_F^2 + \bar{m}^2)^{1/2} + U_V](1 + \frac{1}{3}f_1). \quad (18)$$

Some Landau parameters can be related to the bulk (macroscopic) properties of nuclear matter. Two important examples are the incompressibility K and the symmetry energy β , which are related to the Landau parameters f_0 and f'_0 , respectively [12,47]:

$$K = \frac{3k_F^2}{(k_F^2 + \bar{m}^2)^{1/2}}(1 + f_0), \quad (19)$$

$$\beta = \frac{1}{6} \frac{k_F^2}{(k_F^2 + \bar{m}^2)^{1/2}}(1 + f'_0). \quad (20)$$

We show in Fig. 6 the five Landau parameters obtained in the Dirac-Brueckner calculation with the Bonn A potential. The solid, long-dashed, medium-dashed, short-dashed, and dotted curves correspond to f_0 , f'_0 , g_0 , g'_0 , and f_1 , respectively. The dotted curve with squares represents the results for f_1 based on the Walecka model [48]. It is clearly observed that, while f_0 and f_1 depend strongly on the density of the system, the other three Landau parameters are almost density independent.

The macroscopic properties of the nuclear system, such as the incompressibility K and the symmetry energy β , impose some constraints on the values of the Landau parameters, and further on the bare NN interaction used in the Dirac-Brueckner calculation. It is seen in Eqs. (19) and (20) that, for K and β to be positive, we should have $f_0 > -1$ and $f'_0 > -1$. As we notice in the figure, the value of f'_0 is larger than zero, which leads always to a positive symmetry energy. On the other hand, it can be

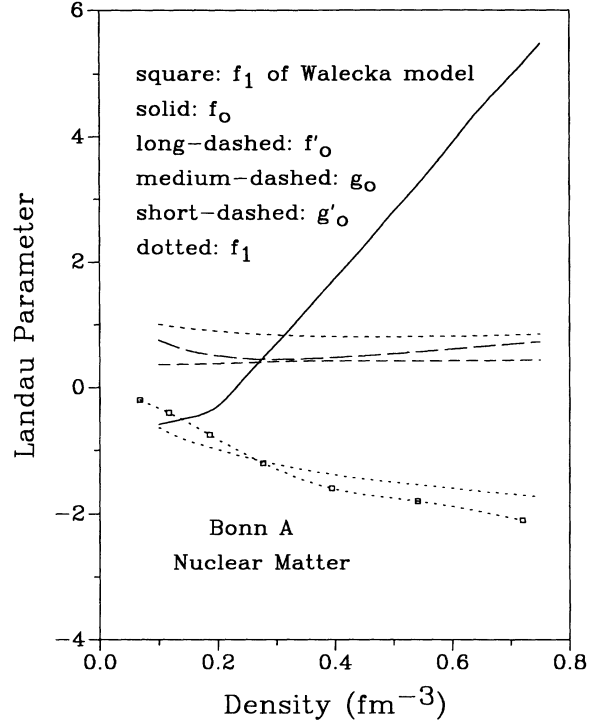


FIG. 6. The variation of the Landau parameters with density. The solid, long-dashed, medium-dashed, short-dashed, and dotted curves correspond to f_0 , f'_0 , g_0 , g'_0 , and f_1 , respectively. The dotted curve with squares is the result for f_1 from the Walecka model [34].

anticipated from the variation of f_0 with density that the value of f_0 obtained in the present calculation with the OBE potential could be less than -1 , if the density of the system is extremely low. Defining the density at which $f_0 = -1$ as critical density, ρ_c , we find that $\rho_c \approx 0.07-0.08 \text{ fm}^{-3}$. The appearance of $f_0 < -1$ at low density should, however, not be considered as a shortcoming of the Dirac-Brueckner approach or the OBE potential used in the calculation. It could actually be identified with the instability of the nuclear system at low density that has recently been observed in heavy-ion reactions [49]. At low density, the system enters the so-called “spinodial region” where its incompressibility is negative and the system becomes unstable. Experimentally it is found that the critical density at which the system enters the spinodial region is about half to two-thirds of the normal density, which is in agreement with our prediction. Physically this instability is due to strong correlations between nucleons when the density is low. Correlated nucleons form clusters which repel each other and make the system fragment.

5. Speed of sound

The principle of causality puts constraints on the nuclear equation of state, or the underlying NN interactions. Especially in Refs. [50–52] it was shown that the widely used empirical Skyrme force violates causality in

extremely dense nuclear matter, when a nonrelativistic treatment for the speed of sound is adopted. This phenomenon of causal violation is also known as superluminosity.

The speed of sound in a nuclear medium, u_1 , in units of the velocity of light is given by [48]

$$u_1^2 = \frac{\partial P}{\partial \epsilon}, \quad (21)$$

where P is the pressure of the system.

In the relativistic treatment, u_1^2 is directly proportional to the incompressibility of nuclear matter. Its explicit expression is [48]

$$u_1^2 = \frac{k_F^2}{3(k_F^2 + \bar{m}^2)^{1/2}[U_V + (k_F^2 + \bar{m}^2)]^{1/2}}(1 + f_0). \quad (22)$$

We show in Fig. 7 the density dependence of the speed of sound in nuclear matter. The solid curve is our result obtained in the Dirac-Brueckner calculation with the Bonn A potential, the dashed curve represents the result of Ref. [48] which is obtained in the mean field theory of the Walecka model, and the dotted curve is the result of Ref. [50] which is derived from the Skyrme force SIII. While in all three cases the speed of sound increases with density, the two phenomenological approaches show a much stronger density dependence. The strong density dependence of the speed of sound with the Walecka model is related to its unrealistically large incompressibility at the saturation point ($K \approx 540$ MeV). Unlike the Walecka model and the Dirac-Brueckner approach which satisfy causality up to the density considered in the present work, the Skyrme force SIII in the nonrelativistic treatment leads to superluminosity already at a density about four times the saturation density.

In Table III we have summarized some important quantities of dense nuclear matter at density $\rho=0.20, 0.40,$ and 0.60 fm^{-3} as predicted in the Dirac-Brueckner

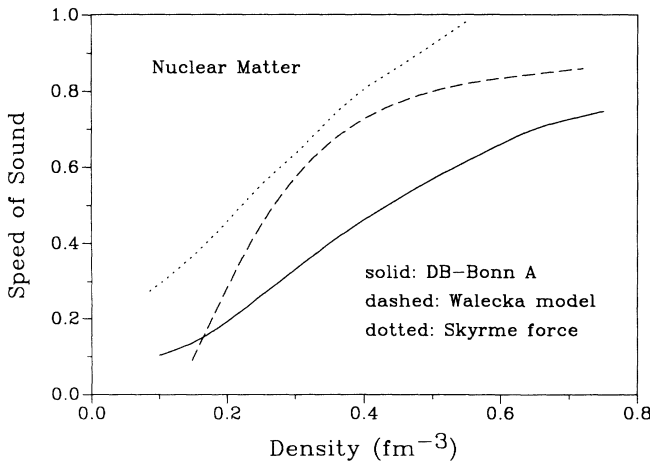


FIG. 7. The variation of the speed of sound (in units of c) in nuclear matter with density. The solid curve is our result; the dashed and dotted curves are the results of Refs. [34] and [36], respectively.

TABLE III. Properties of nuclear matter at high densities as obtained in the Dirac-Brueckner calculation with Bonn A, B, and C potentials.

	$\rho=0.2 \text{ fm}^{-3}$			$\rho=0.4 \text{ fm}^{-3}$			$\rho=0.6 \text{ fm}^{-3}$		
	A	B	C	A	B	C	A	B	C
U_S (MeV)	-389.56	-387.98	-387.43	-532.80	-525.63	-518.86	-585.22	-576.20	-566.79
U_V (MeV)	302.08	305.01	308.06	465.89	467.85	468.60	617.12	618.14	616.84
$U_{s.p.}(\mathbf{p}=0)$ (MeV)	-87.48	-82.92	-79.37	-66.91	-57.78	-50.26	31.80	41.84	50.05
m^*/m	0.678	0.675	0.672	0.504	0.502	0.501	0.343	0.342	0.343
\bar{m}/m	0.585	0.587	0.587	0.433	0.440	0.447	0.377	0.386	0.396
m_L^*/m	0.658	0.660	0.660	0.576	0.581	0.587	0.576	0.581	0.588
\mathcal{E}/A (MeV)	-15.51	-10.72	-8.33	5.61	10.65	14.79	61.77	67.89	72.98
f_0	-0.291	-0.271	-0.266	0.641	0.691	0.675	1.541	1.557	1.520
f_0'	0.250	0.218	0.172	0.244	0.192	0.130	0.306	0.238	0.169
g_0	0.189	0.203	0.194	0.215	0.230	0.225	0.213	0.225	0.230
g_0'	0.445	0.463	0.437	0.413	0.422	0.389	0.408	0.403	0.388

calculations with Bonn A, B, and C potentials. They include Dirac potentials U_S and U_V , single-particle potential $U_{s.p.}(\mathbf{p}=0)$, effective mass m^* , Dirac mass \tilde{m} , Landau mass m_L^* , energy per nucleon, \mathcal{E}/A , and the Landau parameters.

B. Neutron matter

Neutron matter is also a hypothetical system. It can be regarded as extremely asymmetric nuclear matter with an asymmetry parameter $(N-Z)/A=1$. The most significant difference between nuclear matter and neutron matter is the fact that while in the former one quantum state can accommodate four nucleons, in the latter only two neutrons can be accommodated. At the same density, the Fermi momentum of neutron matter is larger than that of nuclear matter. We will present in this subsection our results for properties of neutron matter, in a way parallel to Sec. III A.

1. Single-particle potentials

First we show the density dependence of the Dirac potentials U_S and U_V (Fig. 8). We present three kinds of results corresponding to three different OBE potentials. However, the difference among the three kinds of results is too small to be noticeable on the scale of the figure. This is reasonable since the main difference between the three OBE potentials is in their tensor force strength in the $(T=0)$ 3S_1 - 3D_1 state that does not contribute to the $(T=1)$ neutron-neutron state.

Furthermore in Figs. 9(a) and 9(b) we show the single-particle potential $U_{s.p.}$ as function of the density and as a function of momentum, respectively. In Fig. 9(a) the

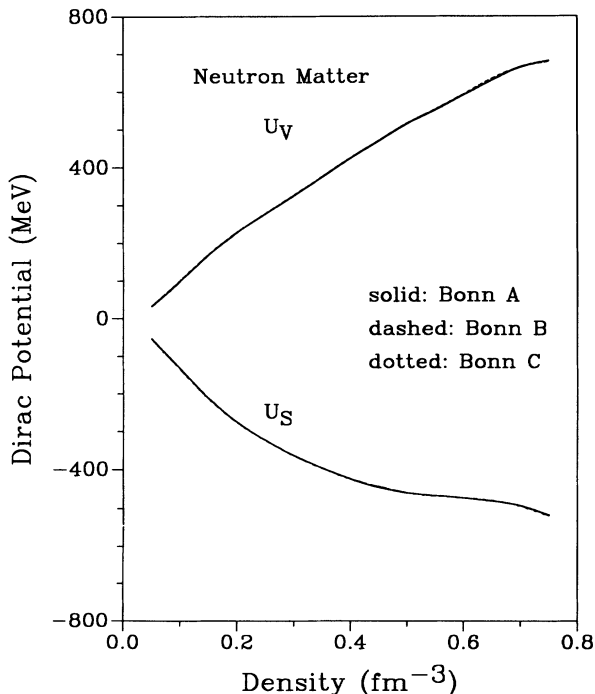


FIG. 8. The same as Fig. 1, but for neutron matter.

solid, dashed, and dotted curves correspond to the potentials of neutrons with momentum 0, 1.35, and 4.05 fm^{-1} , respectively, while in Fig. 9(b) the solid, dashed, and dotted curves represent three cases with neutron density $\rho=0.15, 0.30,$ and 0.45 fm^{-3} , respectively. The variations of these potentials with momentum and density are similar to their counterparts in nuclear matter. The behavior of the Schrödinger-equivalent potential in neutron matter should also be similar to that in nuclear matter.

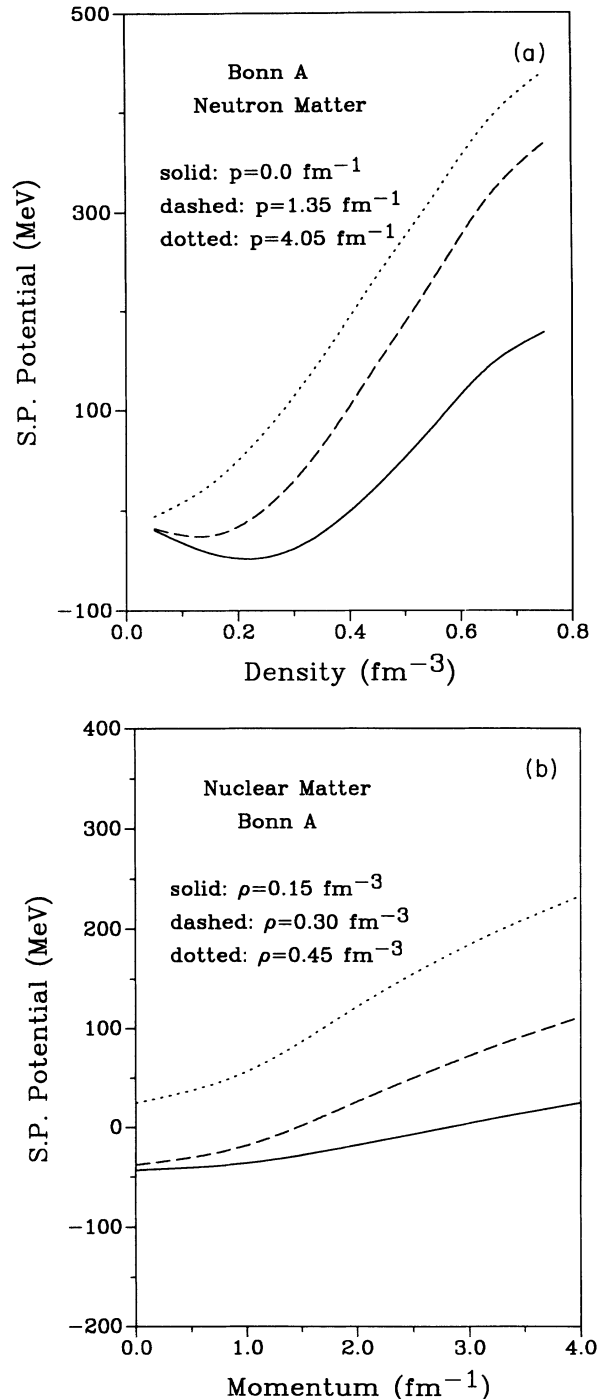


FIG. 9. (a) The same as Fig. 2(a), but for neutron matter. (b) The same as Fig. 2(b), but for neutron matter.

2. Equation of state

The theoretical equation of state of neutron matter is often used in the study of the properties of neutron stars [35,36]. The microscopic equation of state (solid curve) of neutron matter obtained in the present work with the Bonn A potentials is plotted in Fig. 10. Also shown in the figure are the equation of state for neutron matter given in Ref. [35] (dashed curve) which is derived from an improved Walecka model and the equation of state from Ref. [9] (dotted curve) which is obtained in a nonrelativistic variational calculation. There are sizable differences between our microscopic equation of state based on the Dirac-Brueckner approach and the equation of state based on the Walecka model or on the nonrelativistic approach. As in the case of nuclear matter [Fig. 4(b)], our equation of state is stiffer than that of nonrelativistic approach but softer than that of the Walecka model. In further work, we intend to apply our microscopic equation of state to the properties of neutron stars. To do so, the present model should be extended, since there is a difference between pure neutron matter and the actual neutron star matter where many other particles exist.

3. Effective mass

We introduce also three different “effective masses” in neutron matter. The Dirac mass \bar{m} , the effective mass m^* , and the Landau mass m_L^* are presented in Fig. 11 with solid, long-dashed, and short-dashed curves, respectively. Their variation with density is similar to the vari-

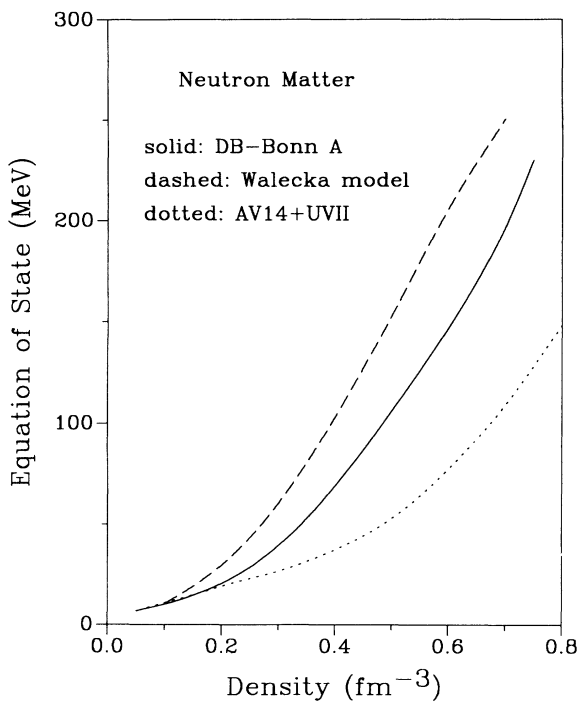


FIG. 10. The same as Fig. 4(b), but for neutron matter. The solid curve represents the present result with the Bonn A potential, while the dashed and dotted curves correspond to the results of the Walecka model [35] and the nonrelativistic calculation [9].

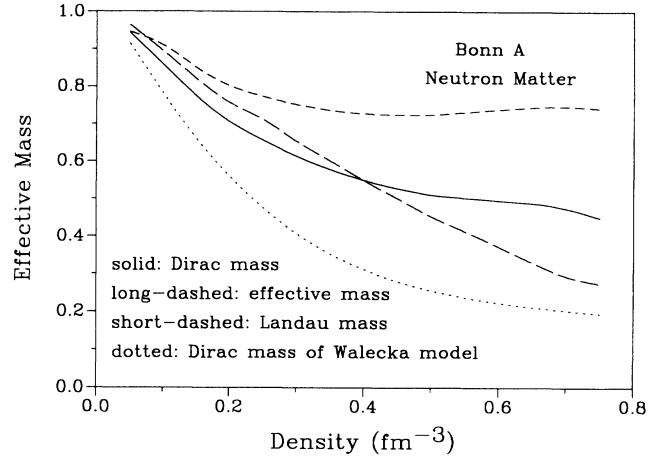


FIG. 11. The same as Fig. 5, but for neutron matter.

ations of their counterparts in nuclear matter. The Landau mass in neutron matter is considerably larger than the one in nuclear matter. m_L^* is proportional to the Fermi momentum which is larger in neutron matter than in nuclear matter, if the densities are the same. Again we notice that the Dirac mass of the Walecka model (dotted curve) [34] decreases much faster with the increasing density.

4. Landau parameters

One can also introduce the Landau parameters for neutron matter. The only difference is the expression for the

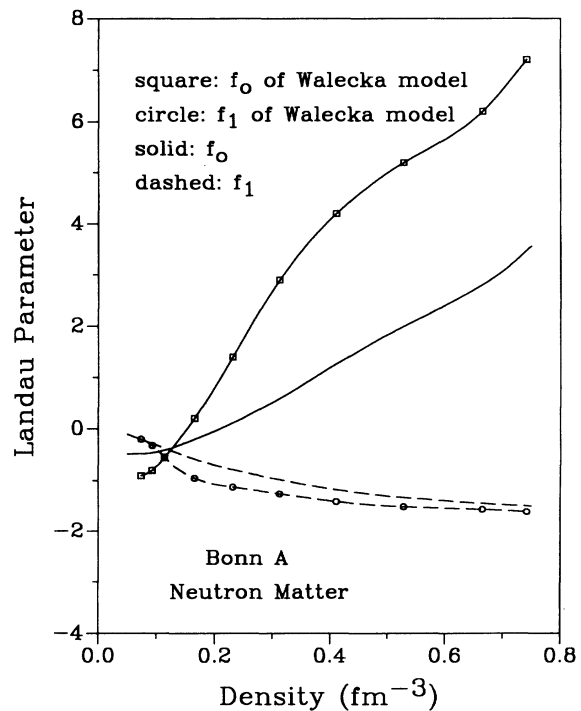


FIG. 12. The Landau parameters f_0 (solid curve) and f_1 (dashed curve) as obtained with the Bonn A potential. Curves with squares and circles correspond to results obtained from the Walecka model [47].

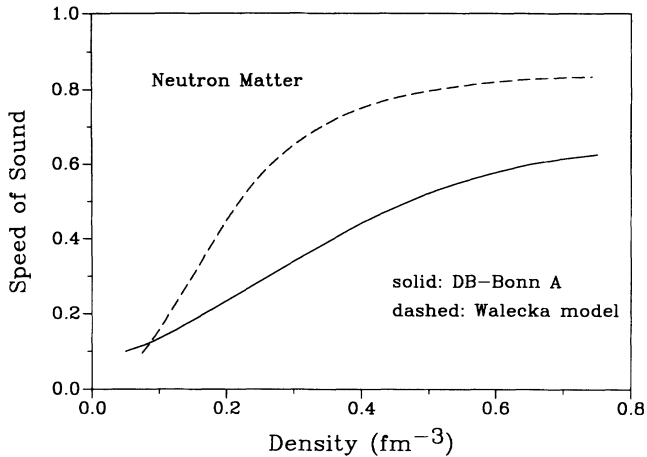


FIG. 13. The same as Fig. 7, but for neutron matter.

inverse density of state. In the neutron matter,

$$C^{-1} = \frac{k_F(k_F^2 + \tilde{m}^2)^{1/2}}{\pi^2}. \quad (23)$$

We show in Fig. 12 two Landau parameters as functions of the density of neutron matter. The solid and dashed curves correspond to the present results for f_0 and f_1 , respectively, while the curves with squares and circles represent the corresponding Landau parameters obtained from the Walecka model [48]. It is observed that f_1 obtained in the microscopic Dirac-Brueckner calculation is in agreement with that obtained in the phenomenological Walecka model (see also Fig. 6). There is, however, a considerable difference between the values of f_0 obtained in the two approaches. The Walecka model predicts in a larger f_0 , since it has a larger incompressibility.

5. Speed of sound

The speed of sound in neutron matter can be obtained with the help of Eq. (21). The result of our calculation is presented in Fig. 13 together with the speed of sound taken from Ref. [48]; they are shown in the figure by solid and dashed curves, respectively. We see a considerable difference between the two results, especially at high density. The difference can again be traced back to the difference in the predictions of the two models for the incompressibility of neutron matter. The incompressibility obtained in the Walecka model is much larger than the one obtained in the present work with Bonn potentials.

IV. SUMMARY AND OUTLOOK

Based on the realistic and relativistic NN interaction of the Bonn group, we performed Dirac-Brueckner calculations which yield an effective NN interaction, the so-called G matrix, in the nuclear medium. Based on this effective interaction we have studied the properties of dense nuclear matter and neutron matter. The important conclusions are the following.

(1) The Bonn A potential, with a weak tensor force strength corresponding to a D -state probability $P_D = 4.5\%$, reproduces quantitatively the empirical saturation properties of nuclear matter. It also leads to a reasonable nucleon effective mass as compared to the empirical value obtained in the nonrelativistic shell or optical model.

(2) The microscopic equations of state of nuclear matter and neutron matter show different behaviors when compared to the widely used equations of state of Skyrme parametrization, the Walecka model, or the nonrelativistic approach. Of particular importance is the fact that our equation of state is softer than that of the Walecka model [34,35] but stiffer than that of the most recent and most sophisticated nonrelativistic calculation [9]. It would now be interesting to apply these microscopic equations of state in the domains of heavy-ion physics and astrophysics. These applications are also connected with the long-pursued goal of understanding nuclear structure and nuclear reactions in terms of the underlying “bare” NN interaction.

(3) The speed of sound obtained in the present calculations increases with density, but at a rate much smaller than the speed of sound obtained from the Walecka model. It can be anticipated that the Bonn potential, when used in the Dirac-Brueckner framework, satisfies causality.

In this paper we have been concerned with symmetric nuclear matter (i.e., equal proton and neutron densities) and pure neutron matter. The properties of asymmetrical nuclear matter (with different proton and neutron densities) are also of interest, especially in the formation of supernovae and black holes. According to the model of prompt explosion [53], an electron-capture process drives the presupernova to an equilibrium state where the proton concentration is $Z/A \approx 1/3$, or asymmetrical parameter $(N-Z)/Z \approx 1/3$, which, depending on the stiffness of this asymmetric nuclear matter, might lead to a supernova or black hole. The extension of the Dirac-Brueckner calculation to the case of asymmetric nuclear matter is straightforward, and the investigation is in progress.

The success of the Dirac-Brueckner calculation for nuclear matter makes it promising to pursue a self-consistent approach for the description of nuclear structure and nuclear reactions in terms of the bare NN interaction. There have been first investigations in which the Dirac-Brueckner approach is applied to nucleon-nucleus scattering using the Bonn potential in the local density approximation [54]. Besides the OBE model used in the present work, we also have a more comprehensive multi-boson-exchange model for the NN interaction which takes into account isobaric degree of freedom explicitly [11,20]. With this model it is possible for us to perform a systematic study of nucleon-nucleus scattering up to incident energies of about 1 GeV.

The development of a self-consistent approach for nucleus-nucleus collisions is also a recent focus [55,56]. Since in our calculation, the G matrix is obtained directly in the nuclear matter rest frame, the present approach can be easily extended to the case of nucleus-nucleus col-

lisions where the c.m. system of the two colliding nuclei shall be used. The main modification on Eq. (5) is the Pauli operator which should represent the Pauli blocking due to two overlapping and time-dependent Fermi spheres [57]. Once we obtain the G matrix, the mean field and the in-medium NN cross section, which are used in the Boltzmann-Uehling-Uhlenbeck equation [26] or

quantum molecular dynamics [27], can be evaluated in a standard way [58].

This work was supported in part by the NSF-Idaho EPSCoR program under Grant No. RII-8902065, the NSF-Physics program under Grant No. 8911040, and the San Diego Supercomputer Center.

-
- [1] K. A. Brueckner, C. A. Levinson, and H. M. Mahmoud, *Phys. Rev.* **95**, 217 (1954).
- [2] H. A. Bethe, *Phys. Rev.* **103**, 1353 (1956).
- [3] J. Goldstone, *Proc. R. Soc. London* **A239**, 267 (1957).
- [4] B. D. Day, *Rev. Mod. Phys.* **39**, 719 (1967); **50**, 495 (1978); *Phys. Rev. C* **24**, 1023 (1981).
- [5] M. Baldo, I. Bombaci, L. S. Ferreira, G. Giansiracusa, and U. Lombardo, *Phys. Rev. C* **43**, 2605 (1991).
- [6] I. Bombaci and U. Lombardo, *Phys. Rev. C* **44**, 1892 (1991).
- [7] R. Jastrow, *Phys. Rev.* **98**, 1479 (1955).
- [8] V. P. Pandharipande and R. B. Wiringa, *Rev. Mod. Phys.* **51**, 821 (1979); B. D. Day and R. B. Wiringa, *Phys. Rev. C* **32**, 1057 (1985).
- [9] R. B. Wiringa, V. Fiks, and A. Fabrocini, *Phys. Rev. C* **38**, 1010 (1986); R. B. Wiringa, *ibid.* **43**, 1585 (1991); R. B. Wiringa, Argonne Report PHY-6919-TH-91.
- [10] K. Kotthoff, R. Machleidt, and D. Schütte, *Nucl. Phys.* **A264**, 484 (1976); K. Holinde and R. Machleidt, *ibid.* **A280**, 429 (1977); M. R. Anastasio, A. Faessler, H. Müther, K. Holinde, and R. Machleidt, *Phys. Rev. C* **18**, 2416 (1978); R. Machleidt and K. Holinde, *Nucl. Phys.* **A350**, 396 (1980).
- [11] R. Machleidt, *Adv. Nucl. Phys.* **19**, 189 (1989).
- [12] M. R. Anastasio, L. S. Celenza, W. S. Pong, and C. M. Shakin, *Phys. Rep.* **100**, 327 (1983).
- [13] R. Brockmann and R. Machleidt, *Phys. Lett.* **149B**, 283 (1984).
- [14] C. J. Horowitz and B. D. Serot, *Phys. Lett.* **137B**, 287 (1984).
- [15] B. ter Haar and R. Malfliet, *Phys. Rev. Lett.* **56**, 1237 (1986); **59**, 1652 (1987).
- [16] B. ter Haar and R. Malfliet, *Phys. Rep.* **149**, 207 (1987).
- [17] L. D. Miller and A. E. S. Green, *Phys. Rev. C* **5**, 241 (1972).
- [18] R. Brockmann and W. Weise, *Nucl. Phys.* **A355**, 365 (1981).
- [19] L. G. Arnold, B. C. Clark, and R. L. Mercer, *Phys. Rev. C* **19**, 917 (1979).
- [20] S. J. Wallace, *Annu. Rev. Nucl. Part. Sci.* **37**, 267 (1987).
- [21] R. Machleidt, K. Holinde, and Ch. Elster, *Phys. Rep.* **149**, 1 (1987).
- [22] R. Brockmann and R. Machleidt, *Phys. Rev. C* **42**, 1965 (1990).
- [23] H. Müther, R. Machleidt, and R. Brockmann, *Phys. Lett. B* **198**, 45 (1987); *Phys. Rev. C* **42**, 1981 (1990).
- [24] N. K. Glendenning, *Nucl. Phys.* **A480**, 597 (1988).
- [25] E. Müller, *J. Phys. G* **16**, 1571 (1990).
- [26] G. F. Bertsch and S. Das Gupta, *Phys. Rep.* **160**, 189 (1988).
- [27] J. Aichelin, *Phys. Rep.* **202**, 235 (1991).
- [28] J. Q. Wu and C. M. Ko, *Nucl. Phys.* **A489**, 810 (1989).
- [29] G. Q. Li, T. Maruyama, D. T. Khoa, S. W. Huang, Y. Lotfy, A. Faessler, and J. Aichelin, *Nucl. Phys.* **A534**, 697 (1991).
- [30] G. Q. Li, D. T. Khoa, T. Maruyama, S. W. Huang, N. Ohtsuka, A. Faessler, and J. Aichelin, *Z. Phys. A* **340**, 271 (1991).
- [31] G. E. Brown, V. Koch, and M. Rho, *Nucl. Phys.* **A535**, 701 (1991).
- [32] J. D. Walecka, *Ann. Phys. (N.Y.)* **83**, 491 (1974).
- [33] C. J. Horowitz and B. D. Serot, *Nucl. Phys.* **A464**, 613 (1987).
- [34] B. D. Serot and J. D. Walecka, *Adv. Nucl. Phys.* **16**, 1 (1986).
- [35] N. K. Glendenning, *Nucl. Phys.* **A493**, 521 (1989).
- [36] F. Weber and M. K. Weigel, *Nucl. Phys.* **A493**, 549 (1989).
- [37] S. Kahana, *Annu. Rev. Nucl. Part. Sci.* **39**, 231 (1989).
- [38] R. H. Thompson, *Phys. Rev. D* **1**, 710 (1970).
- [39] E. E. Salpeter and H. A. Bethe, *Phys. Rev.* **84**, 1232 (1951).
- [40] R. Machleidt, in *Computational Nuclear Physics*, Vol. II, edited by K. Langanke, J. A. Maruhn, and S. E. Koonin (Springer, Heidelberg, 1992).
- [41] M. I. Haftel and F. Tabakin, *Nucl. Phys.* **A158**, 1 (1970).
- [42] Z. Y. Ma, P. Zhu, Y. Q. Gu, and Y. Z. Zhuo, *Nucl. Phys.* **A490**, 619 (1988).
- [43] M. Jaminon and C. Mahaux, *Phys. Rev. C* **40**, 354 (1989).
- [44] M. Brack, C. Guet, and H. B. Hakansson, *Phys. Rep.* **123**, 275 (1985).
- [45] L. S. Celenza and C. M. Shakin, *Relativistic Nuclear Physics: Theory of Structure and Scattering* (World Scientific, Singapore, 1986).
- [46] D. Pines and P. Nozieres, *The Theory of Quantum Liquids* (Benjamin, New York, 1966).
- [47] S. Krewald, K. Nakayama, and J. Speth, *Phys. Rep.* **161**, 103 (1988).
- [48] H. Uechi, *Nucl. Phys.* **A501**, 813 (1989).
- [49] E. Suraud, C. Gregoire, and B. Tamain, *Prog. Part. Nucl. Phys.* **23**, 357 (1989).
- [50] E. Osnes and D. Strottman, *Phys. Lett.* **166B**, 5 (1986).
- [51] R. K. Su, H. Q. Song, and T. T. S. Kuo, *Phys. Rev. C* **37**, 1770 (1988).
- [52] G. Q. Li, *Commun. Theor. Phys. (Beijing)* **14**, 365 (1990).
- [53] E. Baron, J. Cooperstein, and S. Kahana, *Phys. Rev. Lett.* **55**, 126 (1985).
- [54] C. Nuppenau, A. D. MacKellar, and Y. T. Lee, *Nucl. Phys.* **A511**, 525 (1990).
- [55] J. Jaenicke, J. Aichelin, N. Ohtsuka, R. Linden, and A. Faessler, *Nucl. Phys.* **A536**, 201 (1992).
- [56] G. Q. Li, Y. Lotfy, S. W. Huang, and A. Faessler, *J. Phys. G* **18**, 291 (1992).
- [57] T. Izumoto, S. Krewald, and A. Faessler, *Nucl. Phys.* **A341**, 319 (1980).
- [58] G. Q. Li, R. Machleidt, and A. Faessler, in *Proceedings of the Eighth Winter Workshop on Nuclear Dynamics*, Jackson Hole, Wyoming, 1992, edited by W. Bauer *et al.* (World Scientific, Singapore, in press).